Comparison of Derivative Topographic Surfaces of a DEM Generated from Stereoscopic SPOT Images with Field Measurements

Philip T. Giles and Steven E. Franklin

Abstract

A digital elevation model (DEM) derived from SPOT satellite imagery is evaluated for accuracy in elevation and three of its derivative topographic surfaces: slope gradient, incidence value, and profile curvature. The raw DEM surface is observed to contain a systematic pattern of noise, and analysis of semivariance is used to determine an appropriate window size for filtering. Field measurements of slope gradient, incidence value, and profile curvature are used to evaluate the accuracy of the derivative surfaces. Several processing options are employed to maximize the correlation between the surface representations and the field data. For example, with slope gradient measurements the correlation between field and digital values increased from 0.40 using the raw DEM to 0.78 with a custom-filtered DEM, and the standard deviation of differences decreased from 12.5° to 7.6°. The results emphasize the caution that must be used before using the digital elevation model and its derivative topographic surfaces as estimates of the true landscape configuration.

Introduction

Digital elevation models (DEMs) and derivative topographic surfaces are commonly used as a source of topographic information alone (Pike, 1988), for landscape modeling (Moore *et al.*, 1991), as data layers in a GIS (Wiebel and Heller, 1991), and as ancillary data in remote sensing image analysis (Franklin, 1991). In many cases, the accuracy of the DEM and the effect of errors on the application are unknown. Also, the effect of errors in local neighborhood elevations increases with each higher order derivative when common window methods of estimating topographic variables are used. As accurate sets of evaluation data are rare, especially for derivative topographic surfaces, the user of a DEM should be aware that the digital value at a point may have little correlation with the landscape that is being modeled.

Several authors have discussed the importance of evaluating a DEM (Carter, 1988; Li, 1988; Moore *et al.*, 1991). Methods of recognizing and reducing or eliminating errors have been suggested, often based on criteria such as allowable differences in elevation between adjacent points (e.g., Hannah, 1981) or anomalous values in a window (e.g., Felicisimo, 1994). Brown and Bara (1994) used semivariogram analysis to describe the pattern of systematic errors in USGS $7^1/_2$-minute DEMs and to direct the choice of window size for a smoothing filter.

Stereocorrelated DEMs are created from two complementary images such as aerial photographs and, more recently, satellite images. Descriptions of algorithms and the variables affecting accuracy of DEMs produced from satellite images are available elsewhere (for a list, see Sasowsky *et al.* (1992), p. 815). Given the large areas covered by satellite images and the relative ease and speed of automated processing, it is hoped that these DEMs can be used as reliable sources of topographic data for the various applications listed above.

Examples describing the evaluation of derivative topographic surfaces from a DEM created by stereocorrelation of satellite images are uncommon. Sasowsky *et al.* (1992) used two reference DEMs to test the accuracy of slope gradient and aspect estimated with an elevation model derived from stereoscopic 10-m resolution SPOT images. Digitized maps were used to create the reference DEMs in that study, allowing a comparison for every point in the study area. For a DEM produced from a 10-m SPOT stereopair resampled to 30-m pixels, Bolstad and Stowe (1994) used sets of field measurements of elevation, slope gradient, and aspect for evaluation. In both studies, the greatest slope gradient errors were observed to occur in steep areas where the accuracy of elevation values was also poorest.

In this study, a 20-m resolution grid DEM is generated from stereoscopic SPOT images and used to calculate derivative topographic surfaces. The emphasis of this paper is placed on accuracy evaluation of the derivative measures, not on the DEM creation process. For completeness, the accuracy of the elevation surface is tested with topographic map data. For the derivative surfaces of slope gradient, incidence value, and profile curvature, field measurements are employed in accuracy evaluation. Due to the presence of spatially autocorrelated noise in the raw DEM, various smoothing filters are investigated to increase the correlation between the digital surfaces and the field measurements.

Study Area and Data Used

Study Area

The study area is called the Three Guardsmen Upland, located in southwest Yukon Territory (Figure 1). An area approximately 21 km by 21 km was selected, characterized by moderate to high relief with an elevation range of 1300 m (Figure 2). Maximum relief is approximately 1100 m, and there are several steep cliff faces with slope gradients greater than 55°. Vegetation is strongly affected by the elevation gradient, with dense forests at lower elevations changing to bare surfaces on the high mountain tops.

Department of Geography, University of Calgary, Calgary, Alberta T2N 1N4, Canada.

Photogrammetric Engineering & Remote Sensing, Vol. 62, No. 10, October 1996, pp. 1165–1171.

0099-1112/96/6210-1165$3.00/0

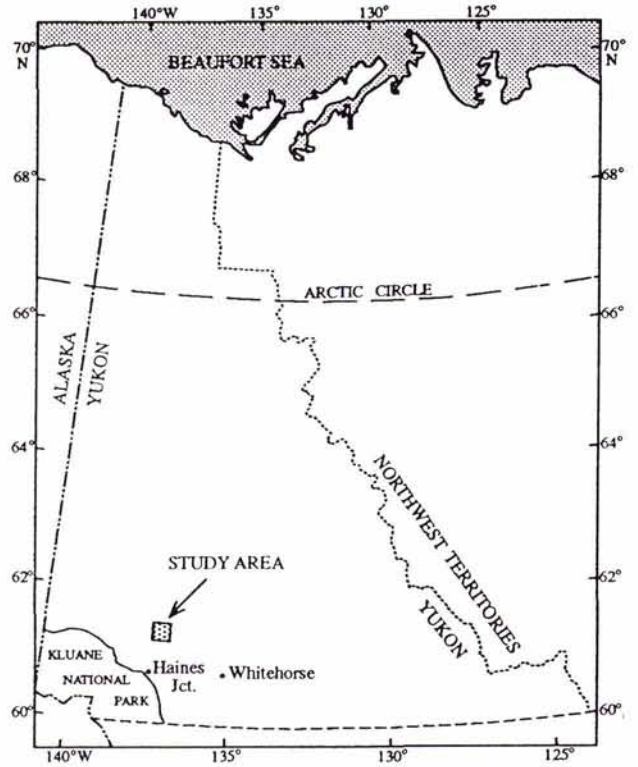

Figure 1. Location of the study area in southwest Yukon Territory.

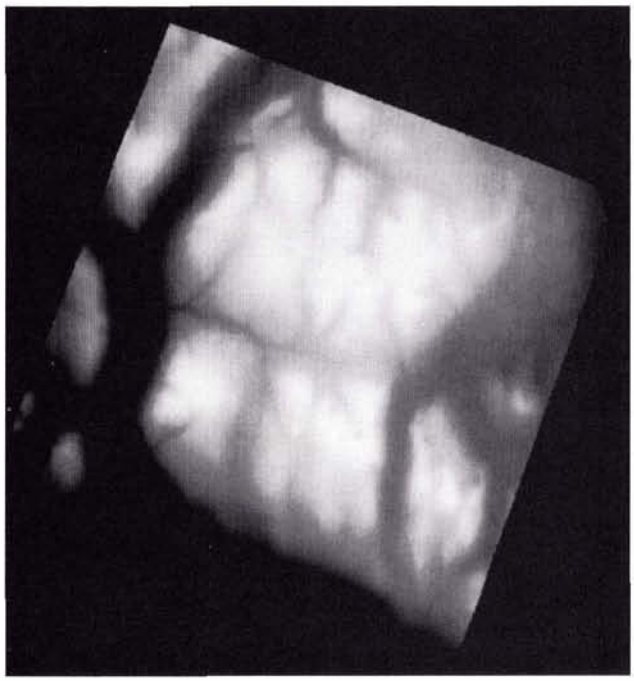

Figure 2. Raw digital elevation model of the study area; lighter areas are higher in elevation. The elevation range represented is approximately 1300 m, and the area of the DEM is 21 km by 21 km. North is towards the top of the frame.

Satellite Images

Stereo SPOT-HRV Multispectral Linear Array (MLA) images with a base-height ratio of 0.63 were obtained. The first image was acquired on 11 August 1989, with a view angle of −27.9°, a sun elevation of 42.6°, and sun azimuth of 160.0°. The second image was acquired on 21 July 1990 with a view angle of 6.0°; the sun elevation and azimuth were 48.9° and 171.1°, respectively.

Digital Elevation Model

An automated DEM generation software package called HI-VIEW (Horler, Inc., 1993) is employed. Corresponding points in both images are required to determine the parallax from which the elevation can be estimated. The method of image correlation used in HI-VIEW has been described in detail previously (Giles *et al.*, 1994). An area matching technique is used, with the user controlling the window size, and the correlation and variance minima required to accept a match. Because it has the greatest contrast of the three available MLA image channels, the near-infrared band was selected for the matching algorithm. The planimetric resolution of the DEM is 20 m; elevation values are recorded with a step size of 0.15 m.

Methodology

Evaluation (Map and Field) Data

Elevation data used for evaluation were extracted from 1:50,000-scale National Topographic Survey maps. A total of 122 points were selected randomly throughout the study area. Field measurements of topographic variables were made in support of a continuing program of geomorphological investigations using digital (elevation and satellite) data. Slope and aspect were measured with an Abney level and a Brunton compass, respectively, at 79 sites.

Profile curvature was measured at 45 locations identified as breaks in slope on the landscape. A series nine or eleven slope angle measurements centered around the break of slope was sufficient to reconstruct a profile. Profile spacing of 20 m was used to correspond to the matrix spacing of the DEM. The value of profile for the central point was found directly by applying orthogonal polynomial regression to the data series. Orthogonal polynomial regression is a method of calculating the value of a derivative at the central point of a data series for a selected order of polynomial. An exact least-squares solution is given by using a unique set of convoluting integers for the given derivative, order of polynomial, and length of series (Steiner *et al.*, 1972). Each convoluting integer is multiplied by the value at the corresponding point in the data series. These products are then summed and divided by the product of the length of the data series multiplied by the interval spacing raised to the power of the derivative order. For these terrain profiles, a fourth-order polynomial was required to represent the terrain surface accurately.

As noted by several other authors, apparent errors in the digital data could be due to errors in the collection of evaluation data, or in the positioning of sites in the digital matrices. Every effort was made to reduce these sources of error; it will be assumed here that the evaluation data are correct and any differences are due to errors in the digital data.

DEM Semivariance Analysis

The raw DEM contains a spatially autocorrelated pattern that appears as apparent pits and hummocks, as shown in Figure 3. Experience in the field, and analysis of air photographs and maps, confirms that this pattern is not representative of

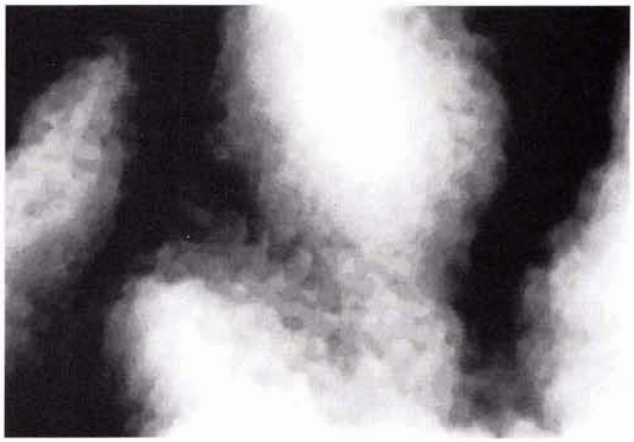

Figure 3. Close-up view of the raw DEM with the pattern of spatially autocorrelated noise. The area shown in this frame is 5 km by 4 km.

the actual land surface. Therefore, semivariance analysis was used to investigate the error pattern and to determine the appropriate window size for filtering. Because elevation is not a stationary variable, the slope gradient surface was used as suggested by Craig (1980).

The familiar equation for semivariance (γ) was employed: i.e.,

$$\gamma(h) = \frac{1}{2n} \sum_{i=1}^{n} [S(x_i) - S(x_i + h)]^2 \quad (1)$$

where h is the lag, n is the number of pairs of sample points separated by h, and $S(x_i)$ is slope at point x_i. At 40 random locations, the semivariance was calculated in the four principal matrix directions (horizontal, vertical, and two diagonals). The range of each semivariogram was determined individually; an average range of 5 1/2 pixels was suggested for this DEM. Anisotropic behavior found by Brown and Bara (1994) was not observed in this case.

Because the sign of slope gradient is ignored (Zevenbergen and Thorne, 1987), the range corresponds to the spatial autocorrelation around both the "crests" (hummocks) and "troughs" (pits) on the surface. Therefore, to remove the error pattern, a window size of 11 was used to span one "wavelength". Methods of error correction that use only the immediate neighbors (3 by 3 window), such as those described by Hannah (1981) and Felicisimo (1994), are inappropriate in this case because it cannot be assumed that the neighboring elevations are correct.

Filtering

A selection of filters was tested to smooth the DEM. Examination of the elevation matrix showed that spot noise existed in addition to the larger error pattern, so a 3 by 3 median filter was first applied to the raw DEM. All subsequent filters used the 3 by 3 median filtered DEM as input. As suggested above, a window size of 11 by 11 was used for the subsequent filters. These included a median filter, a mean filter, and a sigma filter which was specifically designed to smooth a surface while preserving edges (Lee, 1983). Several edge-preserving smoothing filters were evaluated by Abramson and Schowengerdt (1993), and the sigma filter performed the best.

The sigma filter operates by first finding the standard deviation of the values in the window. Then, only those values that lie within a specified number of standard deviations from the current (central) pixel value are included in finding the mean for the window. The range of acceptable values was set to ± 2 standard deviations here. The sigma filter is less sensitive to large errors than the mean filter which averages all values in the window.

Both the median and sigma filters preserve step edges while smoothing. On a flat (non-inclined) surface, a step separates two distinct groups of values. On an inclined surface, the hummocky error pattern described above could resemble steps and be preserved if a flat-lying plane is assumed. Therefore, modified versions of the median and sigma filters were implemented to adapt to the inclined landscape surface. The inclined plane for the current window was approximated by calculating the mean slopes in the vertical and horizontal grid directions. The reference elevation of this plane is arbitrary; here the center pixel was used as the reference elevation. The elevation on the inclined plane for each pixel in the window was calculated as the respective vertical or horizontal mean slope multiplied by the vertical and horizontal grid distance from the central pixel. A matrix of differences for the current window was obtained by subtracting the original elevation values from the corresponding values on the inclined plane. The median and sigma calculations were then conducted on the window of difference values, and the result was added to the center pixel reference elevation value, giving the filtered elevation. These customized filters will be referred to as the inclined median and inclined sigma filters, respectively.

Topographic Variables

Zevenbergen and Thorne's (1987) method of calculating topographic indices from a 3 by 3 window was used. Slope gradient, aspect, and profile curvature are estimated for the central pixel from the neighboring values. Because aspect is a circular variable, this derivative topographic surface was not evaluated directly, but as part of the equation for incidence value. Incidence value (i) varies with aspect and slope gradient and is a ratio of the amount of direct solar radiation received on a surface for instantaneous sun elevation and azimuth conditions (Franklin, 1987). It is calculated using the following equation:

$$i = \cos(\alpha) + \sin(\alpha)*\cot(\beta)*\cos(\theta) \quad (2)$$

where α is slope gradient, β is sun elevation, and θ is the difference between aspect and solar azimuth. Incidence values were calculated using field measurements and digital estimates of slope and aspect. Sun conditions that were in effect during acquisition of the 1990 SPOT image were used for both the field and digital estimates of incidence value.

A second method of calculating profile curvature — orthogonal polynomial regression — was used to compare with the immediate neighbor (3 by 3 window) approach. As with the calculation of profile curvature from the field measurements, the DEM curvature was computed as the second derivative of a fourth-order polynomial fitted to an 11-point series surrounding the central value. This method of calculation serves to smooth variation above the given order of polynomial. The calculation was performed in the four matrix directions for each point, and the curvature was taken as the maximum of the four values.

Results

Elevation

Results of the elevation data accuracy assessment are given in Table 1. As with all of the comparisons, the difference is calculated as the digital value minus the comparison value. The raw DEM actually has more accurate values than any of

TABLE 1. SUMMARY OF RESULTS FOR DIFFERENCES BETWEEN DIGITAL ELEVATION ESTIMATES AND TOPOGRAPHIC MAP VALUES.

Summary of Elevation Errors (Values in m)						
Type of Processing	Maximum	Minimum	Mean	S.D.	R.M.S.E.	Correlation
Raw	53.6	−81.6	0.4	21.6	21.6	0.998
Median 3×3	53.7	−81.6	0.3	21.7	21.7	0.998
Median 11×11	54.9	−82.5	−0.9	22.0	22.0	0.998
Mean 11×11	59.1	−76.8	−0.9	22.1	22.0	0.998
Sigma 11×11	59.0	−76.8	−0.5	21.8	21.8	0.998
Inclined Median 11×11	59.3	−75.2	−0.8	22.0	22.0	0.998
Inclined Sigma 11×11	59.3	−76.1	−0.9	22.0	22.1	0.998

the filtered DEMs. A plot of the evaluation data and the raw DEM values is shown in Figure 4. The root-mean-square error (RMSE) of this DEM compares favorably with other stereocorrelated DEMs reported in the literature (Styles, 1988; Brocklebank and Tam, 1991). Most of the larger differences are located on steeper slopes, or near ridges or peaks that were rounded during the DEM creation process. HI-VIEW has an automatic error detection algorithm for blunder removal which also tends to smooth out these sharp landscape features.

Slope Gradient

The results for slope gradient (Table 2) show a reduction in errors with filtering. There is a very poor relationship between the raw DEM and the field measurements (see also Figure 5a), but the correlation increases to a maximum of 0.78 with the inclined median and inclined sigma filters. The negative mean difference of the filtered DEMs indicates that these surfaces are oversmoothed. This is evident in Figure 5b, which shows that many of the values from the inclined sigma filtered DEM are reasonably accurate, but some of the steeper slopes are not estimated well.

Incidence Value

A pattern similar to the slope gradient results is obtained for the incidence value comparisons (Table 3). Again, the mean, inclined median, and inclined sigma filters produce the lowest standard deviation of errors and the highest correlation values. The improvement in the estimates from the raw DEM to the inclined sigma DEM is seen in the scatterplots in Figure 6.

Profile Curvature

For profile curvature, only the results for the raw DEM and the best of the filtered DEMs are reported because two methods were used. Based on the previous results, the inclined sigma DEM was chosen as the best filtered DEM. Further smoothing before calculating profile curvature gave no improvement, and the results are not reported here.

Using the 3- by 3-window method produced poor results (Table 4a), showing the sensitivity of the calculation to errors in the neighboring values. Values extracted from the raw DEM are completely random (Figure 7a). Different results were obtained with the orthogonal polynomial regression method, which fits a smoothed polynomial function to the data. A moderate relationship is found when the regression method is applied to the inclined sigma DEM (Table 4b). The problem is, however, that smoothing the DEM causes estimates of profile curvature to be much smaller in magnitude than the comparison values (Figure 7b).

Discussion

The raw DEM generated from stereocorrelation of SPOT images is inadequate to represent the surfaces of first- and higher-order derivatives. The elevation surface must be filtered to obtain more accurate estimates of slope gradient, incidence value, and profile curvature. Further improve-

TABLE 2. SUMMARY OF RESULTS FOR DIFFERENCES BETWEEN DIGITAL SLOPE GRADIENT ESTIMATES AND FIELD MEASUREMENTS.

Summary of Slope Gradient Errors (Values in degrees)					
Type of Processing	Maximum	Minimum	Mean	S.D.	Correlation
Raw	32.1	−39.4	0.0	12.5	0.40
Median 3×3	28.0	−37.5	−0.9	11.7	0.47
Median 11×11	20.5	−39.4	−2.3	10.4	0.58
Mean 11×11	6.8	−31.6	−2.5	7.8	0.77
Sigma 11×11	19.2	−31.1	−1.9	9.1	0.67
Inclined Median 11×11	7.9	−28.3	−2.1	7.6	0.78
Inclined Sigma 11×11	6.5	−31.1	−2.2	7.6	0.78

TABLE 3. SUMMARY OF RESULTS FOR DIFFERENCES BETWEEN DIGITAL INCIDENCE VALUE ESTIMATES AND FIELD MEASUREMENTS.

Summary of Incidence Value Errors (Values are dimensionless)					
Type of Processing	Maximum	Minimum	Mean	S.D.	Correlation
Raw	0.75	−0.59	0.03	0.21	0.53
Median 3×3	0.74	−0.56	0.03	0.20	0.59
Median 11×11	0.77	−0.46	0.02	0.17	0.71
Mean 11×11	0.59	−0.23	0.02	0.12	0.87
Sigma 11×11	0.65	−0.23	0.02	0.15	0.79
Inclined Median 11×11	0.56	−0.25	0.01	0.12	0.87
Inclined Sigma 11×11	0.56	−0.24	0.02	0.12	0.88

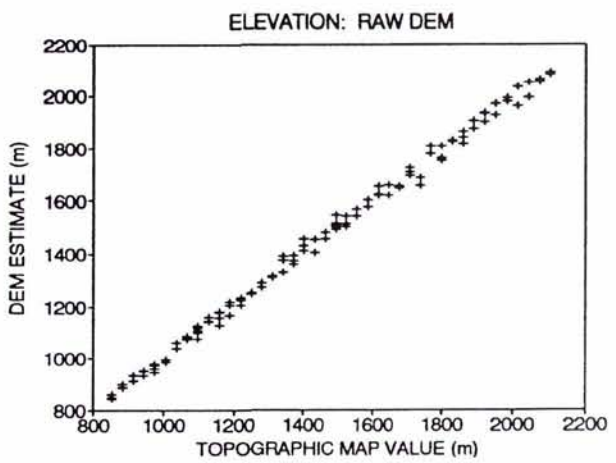

Figure 4. Scatterplot of elevation values extracted from 1:50,000-scale topographic maps against values extracted from the raw DEM.

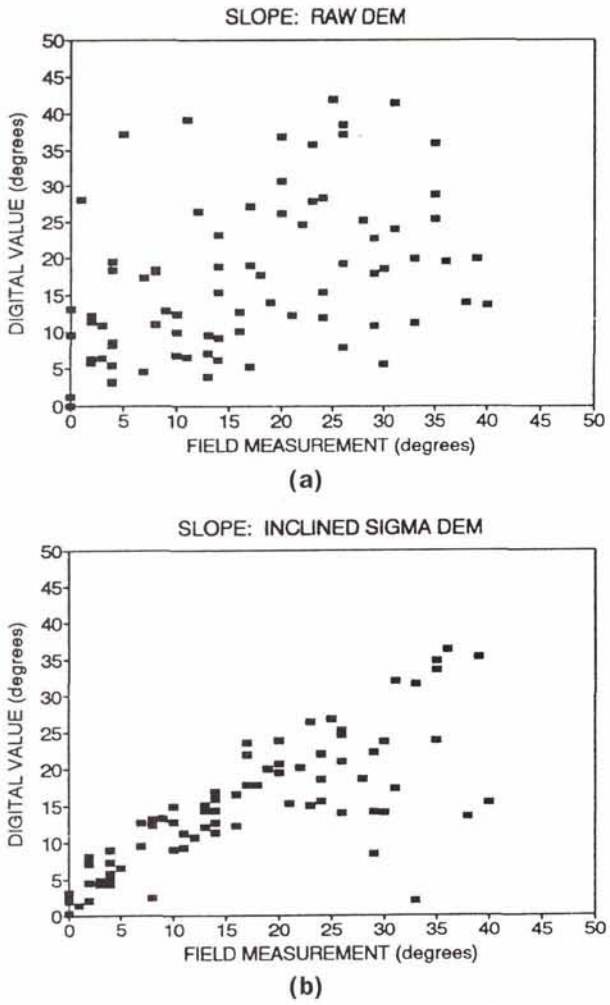

Figure 5. Scatterplots of field measurements of slope gradient against digital values for (a) raw DEM and (b) inclined sigma filter DEM.

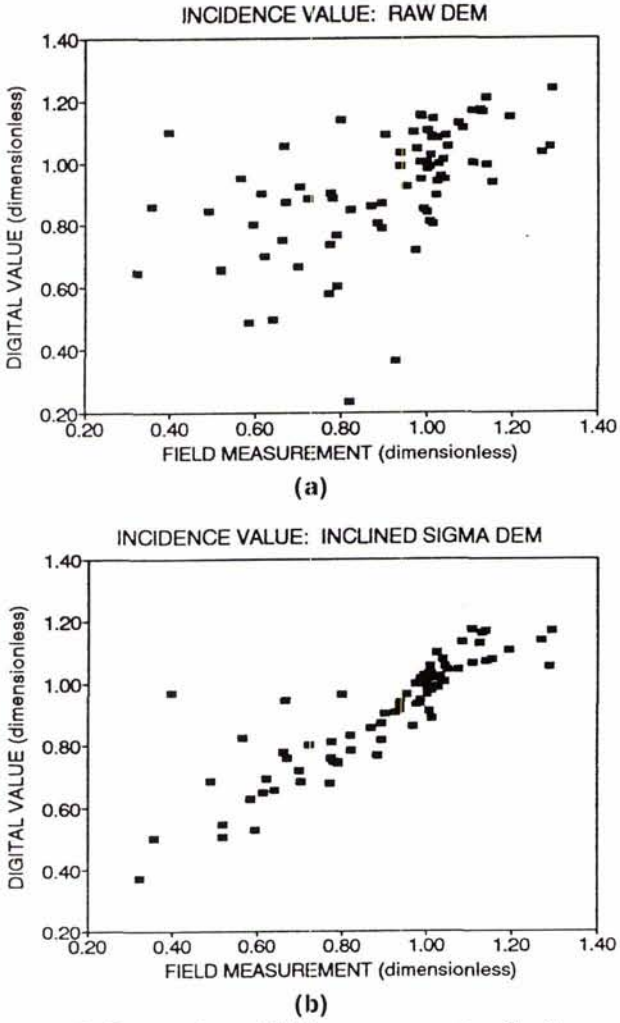

Figure 6. Scatterplots of field measurements of incidence value against digital values for (a) raw DEM and (b) inclined sigma filter DEM.

ments in the characterization of these derivative topographic surfaces at breaks in slope may be possible if a better edge-preserving, smoothing filter can be found.

As the profile curvature results show, it is increasingly difficult to obtain accurate estimates from a DEM for higher-order derivative topographic surfaces. It should be noted that the field locations for measuring profile curvature were intentionally selected at breaks in slope, the parts of a landscape that a smoothed DEM has the most trouble representing accurately. Further field work to measure profile curvature at random locations would be useful for more complete evaluation of this derived surface. Although the magnitude of the digital estimates of profile curvature are too small, it is encouraging to note the presence of at least a moderate correlation in the relationship between filtered digital (inclined sigma) values and field measurements.

Variations in the results can be seen with the different filters employed. For elevation, filtering the raw DEM had a slightly detrimental effect on the estimated values. Summarizing the differences in elevation values is a test of the absolute DEM accuracy, which appears to be controlled by the generation software alone. Filtering improves the relative DEM accuracy, or the relationship between neighboring values, and this is observed in the measures that depend on a local window to calculate a variable. For slope gradient and incidence value, the mean, inclined median, and inclined sigma filters are best suited for this DEM. Although the regular median and sigma filters performed some smoothing, the

TABLE 4. SUMMARY OF RESULTS FOR DIFFERENCES BETWEEN DIGITAL PROFILE CURVATURE ESTIMATES AND FIELD MEASUREMENTS.

Summary of Profile Curvature Value Errors (Values are 1/m)
a) Using a 3×3 processing window

Type of Processing	Maximum	Minimum	Mean	S.D.	Correlation
Raw	0.038	−0.037	−0.0030	0.016	−0.07
Inclined Sigma 11×11	0.016	−0.010	0.0003	0.006	0.47

b) Using orthogonal polynomial regression (11-point series, 4th-order poly.)

Type of Processing	Maximum	Minimum	Mean	S.D.	Correlation
Raw	0.022	−0.016	0.0012	0.009	−0.07
Inclined Sigma 11×11	0.017	−0.010	0.0006	0.006	0.70

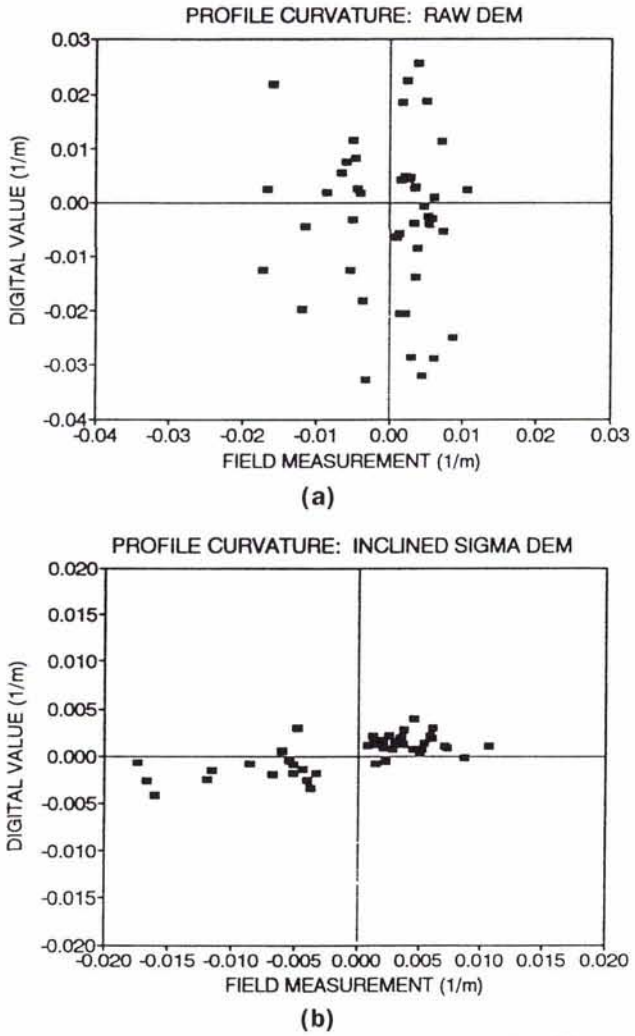

Figure 7. Scatterplots of field measurements of profile curvature against digital values for (a) raw DEM, derived with the 3 by 3 window method; and (b) inclined sigma filter DEM, derived with the orthogonal polynomial regression method. Note the reduction in range of horizontal and vertical scales compared to Figure 7a.

poorer results suggest that steps resulting from the error pattern superimposed on inclined terrain were more likely to be preserved.

Some parts of the landscape that are incorrectly modeled by the DEM cannot be improved with digital processing. As mentioned above, sharp ridges, peaks, and deep valleys are smoothed during creation of the DEM, and accurate reconstruction of these areas is not possible. For example, some of the larger slope gradient errors in Figure 5 are caused by this problem — located near a ridge, the slope gradient is underestimated even after filtering.

Conclusion

The results of this study reinforce the idea that extreme caution must be exercised before a satellite-derived DEM is relied upon to provide estimates of derivative topographic variables. For example, if incorrect values are used as input in process-oriented landscape models, the errors could accumulate to a point where the model is invalid. The main problem, as stated above, is that in most cases accurate comparison data for derivatives of elevation do not exist, and a digital product is used without knowing its accuracy.

After the errors in a raw DEM are characterized, an appropriate method of correction or filtering must be applied before derivatives are calculated. A mean filter and two custom filters that account for the surface inclination in the window produced the best results here. Further work is necessary to find a filter that will smooth the pit and hummock pattern in the DEM, while preserving sharp breaks in slope. This would improve the representation of the landscape near breaks in slope that caused some steeper slopes to be underestimated and the estimated profile curvature values to be too small in magnitude.

Acknowledgments

The first author was supported by a Natural Sciences and Engineering Research Council of Canada Postgraduate Scholarship and a Killam Memorial Scholarship from the University of Calgary. Financial support from the Department of Indian and Northern Affairs Northern Scientific Training Program and from the Canadian Circumpolar Institute for logistical expenses is gratefully acknowledged. Field assistance was provided by Daren Trudeau and Mike Wulder, and valuable comments on the manuscript were given by two anonymous reviewers.

References

Abramson, S.B., and R.A. Schowengerdt, 1993. Evaluation of edge-preserving smoothing filters for digital image mapping, *ISPRS Journal of Photogrammetry and Remote Sensing*, 48(2):2–17.

Bolstad, P.V., and T. Stowe, 1994. An evaluation of DEM accuracy: Elevation, slope, and aspect, *Photogrammetric Engineering & Remote Sensing*, 60(11):1327–1332.

Brocklebank, D.C., and A.P. Tam, 1991. Stereo elevation determination techniques for SPOT imagery, *Photogrammetric Engineering & Remote Sensing*, 57(8):1065–1073.

Brown, D.G., and T.J. Bara, 1994. Recognition and reduction of systematic error in elevation and derivative surfaces from $7^1/_2$-minute DEMs, *Photogrammetric Engineering & Remote Sensing*, 60(2):189–194.

Carter, J.R., 1988. Digital representation of topographic surfaces, *Photogrammetric Engineering & Remote Sensing*, 54(11):1577–1580.

Craig, R.G., 1980. Criteria for constructing optimal digital terrain models, *Applied Geomorphology* (R.G. Craig and J.L. Craft, editors), George Allen & Unwin, London, pp. 108–130.

Felicisimo, A.M., 1994. Parametric statistical method for error detection in digital elevation models, *ISPRS Journal of Photogrammetry and Remote Sensing*, 49(4):29–33.

Franklin, S.E., 1987. Geomorphometric processing of digital elevation models, *Computers and Geosciences*, 13(6):603–609.

———, 1991. Satellite remote sensing of mountain geomorphic surfaces, *Canadian Journal of Remote Sensing*, 17(3):218–229.

Giles, P.T., M.A. Chapman, and S.E. Franklin, 1994. Incorporation of DEMs derived by stereocorrelation of satellite imagery in automated terrain analysis, *Computers and Geosciences*, 20(4):441–460.

Hannah, M.J., 1981. Error detection and correction in digital terrain models, *Photogrammetric Engineering & Remote Sensing*, 47(1): 63–69.

Horler, Inc., 1993. *HI-VIEW Users' Manual Version 3.0*, Horler Information Inc., Ottawa, 200 p.

Lee, J.-S., 1983. Digital image smoothing and the sigma filter, *Computer Vision, Graphics, and Image Processing*, 24(2):255–269.

Li, Z., 1988. On the measure of digital terrain model accuracy, *Photogrammetric Record*, 12(72):873–877.

Moore, I.D., R.B. Grayson, and A.R. Ladson, 1991. Digital terrain modelling: A review of hydrological, geomorphological, and biological applications, *Hydrological Processes*, 5(1):3–30.

Pike, R.J., 1988. The geometric signature: Quantifying landslide-terrain types from digital elevation models, *Mathematical Geology*, 20(5):491–511.

Sasowsky, K.C., G.W. Petersen, and B.M. Evans, 1992. Accuracy of SPOT digital elevation model and derivatives: Utility for Alaska's North Slope, *Photogrammetric Engineering & Remote Sensing*, 58(6):815–824.

Steiner, J., Y. Termonia, and J. Deltour, 1972. Comments on smoothing and differentiation of data by simplified least square procedure, *Analytical Chemistry*, 44(11):1906–1909.

Styles, P.J., 1990. *The Application of Stereoscopic SPOT-HRV Data and DEMs to Geomorphological Mapping*, unpublished PhD thesis, Department of Geography, University of Reading, 303 p.

Weibel, R., and M. Heller, 1991. Digital terrain modelling, *Geographical Information Systems* (D.J. Maguire, M.F. Goodchild, and D.W. Rhind, editors), Longman Scientific & Technical, New York, Chapter 19, pp. 269–297.

Zevenbergen, L.W., and C.R. Thorne, 1987. Quantitative analysis of land surface topography, *Earth Surface Processes and Landforms*, 12(1):47–56.

(Received 17 November 1994; accepted 4 May 1995; revised 25 July 1995)

Forthcoming Articles

Michael Abrams, Remo Bianchi, and Dave Pieri, Revised Mapping of Lava Flows on Mount Etna, Sicily.

M. Aniya, H. Sato, R. Naruse, P. Skvarca, and G. Casassa, The Use of Satellite and Airborne Imagery to Inventory Outlet Glaciers of the Southern Patagonia Icefield, South America.

Ling Bian and Eric West, GIS Modeling of Elk Calving Habitat in a Prairie Environment with Statistics.

Georges Blaha, Accuracy of Plates Calibrated by an Automatic Monocomparator.

M. Les Bober, Duncan Wood, and Raymond A. McBride, Use of Digital Image Analysis and GIS to Assess Regional Soil Compaction Risk.

Gerardo Bocco and Hugo Riemann, Quality Assessment of Polygon Labeling.

Michel Boulianne, Clément Nolette, Jean-Paul Agnard, and Martin Brindamour, Hemispherical Photographs Used for Mapping Confined Spaces.

Timothy L. Bowers and Lawrence C. Rowan, Remote Mineralogic and Lithologic Mapping of the Ice River Alkaline Complex, British Columbia, Canada, Using AVIRIS Data.

Stefan H. Cairns, Kenneth L. Dickson, and Samuel F. Atkinson, An Examination of Measuring Selected Water Quality Trophic Indicators with SPOT Satellite HRV Data.

Ronald J. Duhaime, Peter V. August, and William R. Wright, Automated Vegetation Mapping Using Digital Orthophotography.

Christopher D. Elvidge, Kimberly E. Baugh, Eric A. Kihn, Herbert W. Kroehl, and *Ethan R. Davis,* Mapping City Lights with Nighttime Data from the DMSP Operational Linescan System.

Patricia G. Foschi and Deborah K. Smith, Detecting Subpixel Woody Vegetation in Digital Imagery Using Two Artificial Intelligence Approaches.

Jay Gao and Stephen M. O'Leary, The Role of Spatial Resolution in Quantifying Suspended Sediment Concentration from Airborne Remotely Sensed Data.

Greg G. Gaston, Peggy M. Bradley, Ted S. Vinson, and Tatayana P. Kolchugina, Forest Ecosystem Modeling in the Russian Far East Using Vegetation and Land-Cover Regions Identified by Classification of GVI.

Clyde C. Goad and Ming Yang, A New Approach to Precision Airborne GPS Positioning for Photogrammetry.

Qizhong Guo and Norbert P. Psuty, Flood-Tide Deltaic Wetlands: Detection of Their Sequential Spatial Evolution.

Collin G. Homer, R. Douglas Ramsey, Thomas C. Edwards, Jr., and Allan Falconer, Landscape Cover-Type Mapping Modeling Using a Multi-Scene Thematic Mapper Mosaic.

Pamela E. Jansma and Harold R. Lang, Applications of Spectral Stratigraphy to Upper Cretaceous and Tertiary Rocks in Southern Mexico: Tertiary Graben Control on Volcanism.

Steven T. Knick, John T. Rotenberry, and Thomas J. Zarriello, Supervised Classification of Landsat Thematic Mapper Imagery in a Semi-Arid Rangeland by Nonparametric Discriminant Analysis.

Jacek Komorowski-Blaszczynski, Landform Characterization with Geographic Information Systems.

Miklos Kovats, A Large-Scale Aerial Photographic Technique for Measuring Tree Heights on Long-Term Forest Installations.

Sunil Narumalani, John R. Jensen, Shan Burkhalter, John D. Althausen, and Halkard E. Mackey, Jr., Aquatic Macrophyte Modeling Using GIS and Logistic Multiple Regression.

Paul Pope, Ed Van Eeckhout, and Cheryl Rofer, Waste Site Characterization through Digital Analysis of Historical Aerial Photographs.

Elijah W. Ramsey III, Dal K. Chappell, and Dan G. Baldwin, AVHRR Imagery Used to Identify Hurricane Damage in a Forested Wetland of Louisiana.

R.D. Spencer, M.A. Green, and P.H. Biggs, Integrating Eucalypt Forest Inventory and GIS in Western Australia.

M.D. Tomer, J.L. Anderson, and J.A. Lamb, Assessing Corn Yield and Nitrogen Uptake Variability with Digitized Aerial Infrared Photographs.

A.P. van Deventer, A.D. Ward, P.H. Gowda, and J.G. Lyon, Using Thematic Mapper Data to Identify Contrasting Soil Plains and Tillage Practices.

James D. Wickham, Robert V. O'Neill, Kurt H. Ritters, Timothy G. Wade, and K. Bruce Jones, Sensitivity of Selected Landscape Pattern Metrics to Land-Cover Misclassification and Differences in Land-Cover Composition.

Eric A. Williams and Dennis E. Jelinski, On Using the NOAA AVHRR "Experimental Calibrated Biweekly Global Vegetation Index."

Paul A. Wilson, Rule-Based Classification of Water in Landsat MSS Images Using the Variance Filter.

Zhangshi Yin and T.H. Lee Williams, Obtaining Spatial and Temporal Vegetation Data from Landsat MSS and AVHRR/NOAA Satellite Images for a Hydrologic Model.

Ding Yuan, A Simulation Comparison of Three Marginal Area Estimators for Image Classification.

November 1996
Special Issue on Geographic Information Systems

Thomas R. Allen, Spatial and Compositional Pattern of Alpine Treeline, Glacier National Park, Montana.

P. Gong, R. Pu, and J. Chen, Mapping Ecological Land Systems and Classification Uncertainties from Digital Elevation and Forest Cover Data Using Neural Networks.

Molly B. Sperduto and Russell G. Congalton, Predicting Rare Orchid (Small Whorled Pogonia) Habitat Using GIS.

Jeffrey A. Hepinstall, Lloyd P. Queen, and Peter A. Jordan, Application of a Modified Habitat Suitability Index Model for Moose.

Jiang Zhou and Daniel L. Civco, Using Genetic Learning Neural Networks for Spatial Decision Making in GIS.

Peter F. Fisher, Extending the Applicability of Viewsheds in Landscape Planning.

Rick L. Lawrence, Joseph E. Means, and William J. Ripple, An Automated Method for Rapidly Digitizing Color Thematic Maps.

R. Gavin McGhie, A Comprehensive Managed Areas Spatial Database for the Conterminous United States: Procedures, Problems, and Relevant Issues Encountered in Compiling and Integrating Multiple Data Sources.